THE JOURNAL OF PHYSICAL CHEMISTRY C

Article

pubs.acs.org/JPCC

Dominance of Surface Barriers in Molecular Transport through Silicalite-1

Andrew R. Teixeira, Chun-Chih Chang, Timothy Coogan, Ross Kendall, Wei Fan,* and Paul J. Dauenhauer*

Department of Chemical Engineering, University of Massachusetts Amherst, Amherst, Massachusetts 01003, United States

Supporting Information

ABSTRACT: Development of microporous materials with hierarchical structures of both micro/mesopores leads to molecular transport at nanometer length scales. For novel microporous materials including three-dimensionally ordered mesoporous imprinted (3DOm-i) zeolites and zeolite nanosheets, particle dimensions are below 35 nm resulting in surface-dominated structures. At the same time, the existence of surface-controlled mass transport including undefined "surface barriers" has been observed to reduce apparent diffusivity of hydrocarbons by orders of magnitude. This paper systematically characterizes cyclohexane transport in silicalite-1 by zero length chromatography (ZLC) to determine apparent diffusivity varying over 3 orders of magnitude in particles ranging from 35 nm to 3 μm. Three proposed mechanisms for surface barriers including surface pore narrowing, surface pore blockage, or surface desorption are evaluated by comparison with particle-size/diffusivity data. It is concluded that transport control in small particles was likely due to either pore narrowing at the surface or an extension of the diffusional length scale near the surface due to total pore blockages

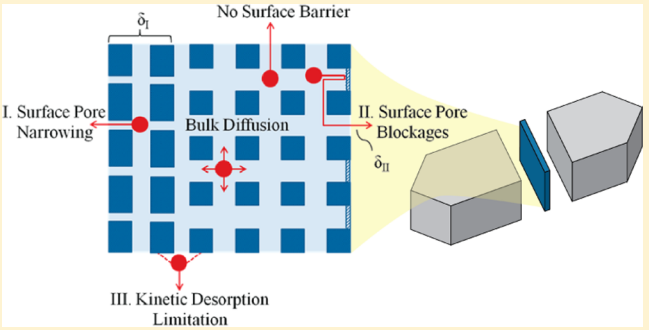

1.0. INTRODUCTION

Zeolites have been synthesized at laboratory and industrial scales for nearly half a century for their catalytic, absorptive, and separative properties. Currently, they are critical for catalytic upgrading of petrochemicals and fuels and have been adapted for use in the upgrading and separation of biofuels. Synthesis of zeolite particles has advanced to the extent that allows for fine control of microporous structure, with well-defined pore networks (d_{pore} < 2 nm) and tunable strength of active sites. The combination of design parameters allows zeolite optimization for targeted applications, controlling molecular diffusion, reactivity, and absorption capacity.[1−4]

For catalytic reactions in microporous materials, molecules diffuse into the pore network, react at the active site, and diffuse out of the pores.[5] To maximize turnover frequency, synthesis of new microporous materials aims to eliminate the contribution of mass transport to the overall conversion rate. One approach is to synthesize zeolite nanocrystals, which have been achieved by precisely controlling nucleation and crystal growth processes. For example, silicalite-1 particles with MFI zeolite topology have recently been synthesized in uniform sizes as small as 62 nm.[6] An emerging approach to faster intraparticle mass transport is to introduce secondary mesoporosity in microporous materials resulting in reduced transport length scales. Hard templating methods have allowed for the synthesis of ordered mesoporous zeolites with close-packed zeolite particles as small as 20 nm.[7,8] The soft templating method has also led to hierarchical zeolites with auxiliary mesoporosity.[9,10] More recently, Tsapatsis and co-workers have developed a synthesis method for pillared zeolite materials consisting of a single unit cell layer.[11] By decreasing transport length scales to a single unit cell, the time scale for diffusion becomes negligibly small in accordance with the square of the particle/sheet size ($\tau = R^2/D$). However, the benefit of hierarchical pore networks on microporous diffusion has yet to be quantified.

Despite decades of study on diffusion in zeolites,[5,12−16] characterization of diffusion in microporous materials remains a significant technical challenge.[17−19] In general, macroscopic methods that measure the apparent/transport diffusivity (e.g., zero length chromatography, gravimetric, frequency response, interference microscopy) predict diffusivities that are orders of magnitude less than those that measure on a microscopic scale (e.g., quasielastic neutron scattering, pulsed field gradient−nuclear magnetic resonance), which measure the tracer/self-diffusivity. Though the relative trend in measured diffusivity values often demonstrates the same activation energies, differences in predicted diffusivities vary as much as 3 orders of magnitude.[5,18,20−23] As a result, this variation has been the topic of significant debate in the literature, with specific questions being raised as to whether the differences are due to synthesis methods, adsorbate loading/concentration, or surface effects.[17,18,23−29]

Received: September 6, 2013
Revised: November 12, 2013
Published: November 13, 2013

   dx.doi.org/10.1021/jp4089595 | J. Phys. Chem. C 2013, 117, 25545−25555

It is proposed that discrepancies in apparent diffusivity result from the variation of length scales between the techniques, with the microscopic methods often measuring over just a few lattice cells.[5,18] Evidence for variation across measurement length scales has led to the idea of hindered transport in smaller particles by introducing a second transport limitation resulting from internal crystal grain boundaries, surface pore restrictions, or total pore blockages. The origins of these ideas are examined further in the Discussion section of this manuscript.

In this work, we aim to characterize the potential second transport limitation within zeolites by carefully controlling diffusional length scales and measuring the temperature-activated apparent diffusion coefficients. For the first time, a complete set of silicalite-1 particles are synthesized with characteristic length scales varying across 3 orders of magnitude, and apparent diffusivity is characterized for each particle. This comprehensive approach allows for experimental assessment of various theories presented in the literature regarding the origin of surface barriers, including surface desorption, pore restriction, and pore blockage.

2.0. MATERIALS AND METHODS

Seven samples of silicalite-1 were synthesized, as summarized in Table 1. Three-dimensionally ordered mesoporous-imprinted (3DOm-i) silicalite-1 with a primary particle size of 35 nm was synthesized according to Fan et al.[7] In short, the 3DOm carbon replica was first synthesized from 35 nm silica nanoparticles, and mesoporous silicalite-1 was synthesized and confined in the voids of the carbon template by using steam-assisted crystallization (SAC). Structure-directing agent (SDA) solution was generated by mixing 3.5 μL of 10 M sodium hydroxide (NaOH, 98%, Aldrich) solution, 1.07 g of tetrapropylammonium hydroxide solution (TPAOH, 40%, Alfa Aesar), 1.25 mL of ethanol (200 proof, Fisher), and deionized water. In a glass vial, 0.3 mL of the SDA solution was introduced into 0.1 g of carbon to match the pore volume in the carbon material. The mixture was left in a fume hood until full evaporation of ethanol was achieved. To the carbon−SDA mixture, 0.15 mL of tetraethylorthosilicate (TEOS, 98%, Alfa Aesar) was added. The glass vial containing carbon mixture was sealed in a Teflon-lined stainless steel autoclave with 3 g of DI water in the vessel without direct contact with the solid mixture. After three hours aging at room temperature, the bomb was put into a preheated 408 K convection oven for two days. The carbon/silicalite-1 composite was washed by filtration and dried in a 373 K oven overnight.

Table 1. Silicalite-1 Particle Size Characterization

nominal crystal size	length[a] (nm)	width[a] (nm)	height[a] (nm)	R^b (nm)	error[c] (nm)
3 μm	7680	4120	1550	1800	79
1 μm	1110	730	337	324	16.7
500 nm	659	590	256	231	8.1
300 nm	328	324	188	136	3.07
200 nm	222	197	125	88	3.21
80 nm	118	83.3	61.5	42.3	1.84
3DOm-i	-	-	-	17.5[d]	-

[a]Measured average from SEM. [b]$R = (lwh)^{1/3}$. [c]95% confidence interval. [d]Determined from template.

Silicalite-1 of different particle sizes ranging from 80 nm to 1 μm was synthesized based on published work.[6] First, TPAOH solution, TEOS, and water were mixed in a Teflon vessel and aged at 353 K for one day while stirring. The composition of the gel was SiO_2:0.25 TPAOH:xH_2O, where x = 11, 38, 60, 100, and 400, which corresponds to a nominal size of 80, 200, 300, 500 nm, and 1 μm, respectively. The resulting gel was charged into a Teflon-lined stainless steel autoclave and heated at 443 K for one day. The product was washed by centrifugation until the pH of the supernatant was below nine. The 3 μm silicalite-1 sample was made according to Agger et al.[30] TEOS was added into a solution of tetrapropylammonium bromide (TPABr, 98%, Adrich) and NaOH, and the mixture was allowed to age at 323 K for eight days. The composition of the gel was SiO_2:0.1TPABr:0.05Na_2O:4EtOH:98H_2O. The aged mother gel was then heated in a Teflon-lined stainless steel autoclave at 408 K for 50 h. The product was washed with a copious amount of DI water and dried in a 373 K oven overnight. The carbon template for 3DOm-i silicalite-1 and the organic structure directing agent occluded in the crystal framework were removed via calcination at 873 K for 24 h with a ramping rate of 3 K/min.

Crystallinity and phase of the porous materials were characterized by powder X-ray diffraction on a diffractometer (X′Pert Pro, PANalytical) with Cu K_α radiation. The morphology and sizes of the crystals were studied by scanning

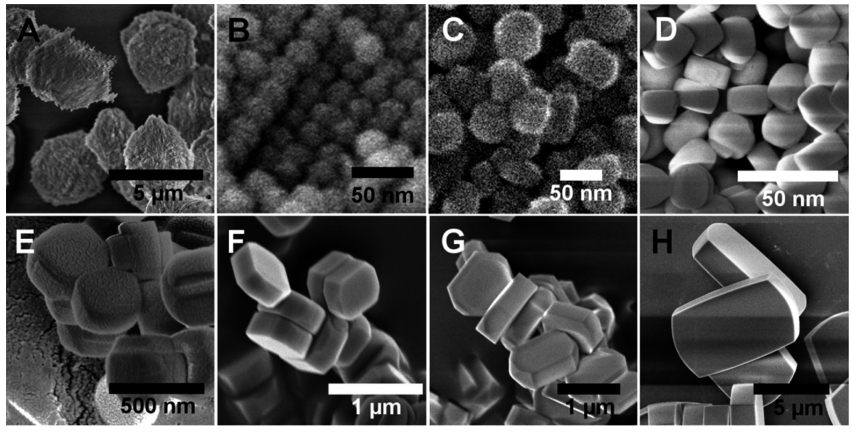

Figure 1. SEM images of silicalite-1 particles, as synthesized. Nominal sizes (A & B) 3DOm-i, (C) 80 nm, (D) 200 nm, (E) 300 nm, (F) 500 nm, (G) 1 μm, and (H) 3 μm.

dx.doi.org/10.1021/jp4089595 | J. Phys. Chem. C 2013, 117, 25545−25555

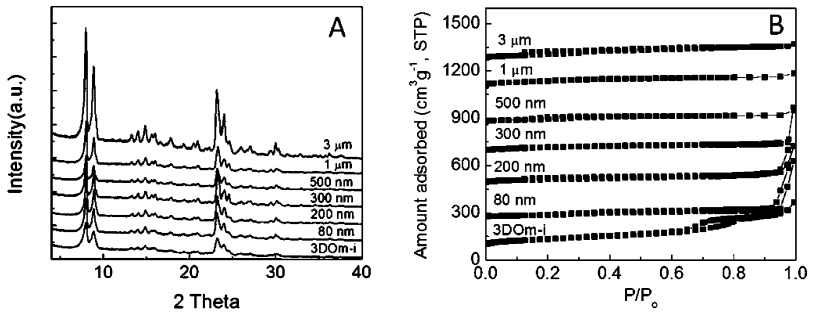

Figure 2. Silicalite-1 characterization. (A) XRD patterns for different sizes of silicalite-1 and 3DOm-i silicalite-1 particles synthesized in this study. (B) N_2 sorption isotherms for different sizes of silicalite-1 and 3DOm-i silicalite-1. The curves were shifted 200 cm^3/g in step. 3DOm-i silicalite-1 shows existence of mesopores, while other isotherms reveal the typical microporous materials nature.

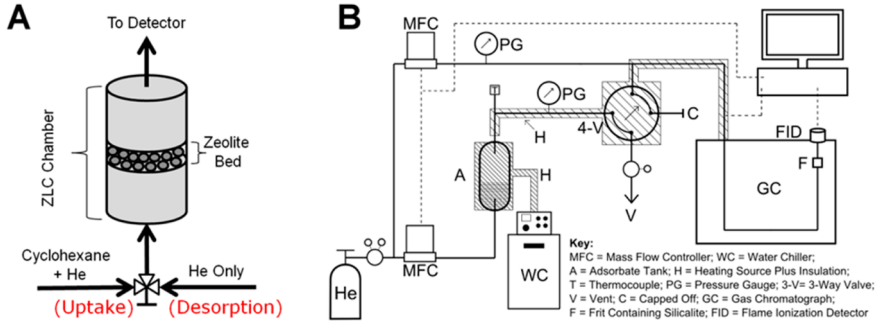

Figure 3. (A) Overview of the ZLC method. A zeolite sample is packed into a 1/4 in. isothermal chamber, and cyclohexane vapor is passed over it for two hours. A valve is switched, and a pure helium stream flows over the material allowing the transient effluent to be monitored. (B) Experimental schematic of the ZLC setup.

Table 2. Zeolite Diffusion Models[a]

	model	BC at surface	L	$D_{app,0}$
-	base	$-D\left.\frac{\partial q}{\partial r}\right\|_R = \frac{FR}{3KV_s}q_R = \frac{FR}{3V_s}c$	$L = \frac{\tau_{Diff}}{\tau_{washout}} = \frac{1}{3}\frac{F}{KV_s}\frac{R^2}{D}$	D_0
I	surface resistance (pore narrowing)	$-D\left.\frac{\partial q}{\partial r}\right\|_R = k(q_R - q_{surf}) = \frac{FR}{3V_s}c = \frac{FR}{3KV_s}q_{surf}$	$L' = \frac{\tau_{diff}}{\tau_{washout} + \tau_{surf}} = \frac{R^2/3D}{KV_s/F + R/k_s}$	$R^2\left[\frac{(R-\delta_I)^2}{D_0} + \frac{\delta_I^2}{D_{s,0}}\right]^{-1}$
II	pore blockage	same as base	same as base	$D_0\left[1 + \left(\frac{\delta_{II}}{R}\right)^2\right]^{-1}$
III	kinetic desorption	$-D\left.\frac{\partial q}{\partial r}\right\|_R = \frac{k_{des}R}{3}q_R = \frac{FR}{3V_s}c$	$L'' = \frac{\tau_{diff}}{\tau_{des}} = \frac{R^2/3D}{1/k_{des}}$	$\frac{k_{des,0}D_0}{k_{des,0}\exp\left(\frac{E_{Diff}-E_{app}}{\mathcal{R}T}\right) + \frac{D_0}{R^2}\exp\left(\frac{-\Delta H_{ads}-E_{app}}{\mathcal{R}T}\right)}$

[a]Boundary conditions, dimensionless fitting parameter L, and apparent Arrhenius pre-exponential $D_{app,0}$ are presented for the four mass transfer models describing pure intracrystalline diffusion (base) and three mechanistic derivations of surface barriers.

electron microscopy (Magellan 400 (FEI) or 6320JXV (JEOL)). Samples were spread on carbon tape and coated with Pt prior to being investigated with scanning electron microscopy at an acceleration voltage of 3.0 kV with a stage bias of 500 V if applicable. Larger particles (>200 nm) exhibited "plate" or "coffin" geometries, while smaller particles were more spherical, as shown in Figure 1. N_2 adsorption−desorption characterization was carried out on an automated gas sorption analyzer (Autosorb iQ, Quantachrome) at 77 K after outgassing at 473 K under vacuum until the pressure rise in the cell was less than 25 mTorr/min.

Figure 2A shows the XRD patterns for different sizes of silicalite-1 and 3DOm-i silicalite-1. All samples exhibit typical patterns for the MFI topology without indication of crystalline impurities. From the N_2 sorption isotherms (Figure 2B), typical type I isotherms for microporous materials are observed for all samples, with the exception of the 3DOm-i silicalite-1. A steep increase at high relative pressures for small silicalite-1 particles is due to the interparticle voids and becomes less prominent in larger crystals. Mesoporosity shown for 3DOm-i silicalite-1 originated from the interstices of the ordered packing structure of 35 nm primary MFI spheres. Micropore volume analysis obtained from the *t*-plot method gives micorpore volumes of 0.10−0.13 cm^3/g for all samples, confirming the high quality of the crystals examined in this work.

Experimental diffusion data were collected using the zero length chromatography (ZLC) technique developed by Eić and Ruthven[31] and extensively applied to measure diffusion in microporous materials.[32−42] The ZLC method has been developed for both one-dimensional (slab) and three-dimensional (spherical) pore network geometries.[43] As depicted in Figure 3, a saturated cyclohexane vapor stream (2.3 Torr) flows over an isothermal monolayer of porous solid (∼5−6 mg) held in place by two porous frits. The effluent is monitored online at

dx.doi.org/10.1021/jp4089595 | J. Phys. Chem. C 2013, 117, 25545−25555

300 Hz with a flame ionization detector. Uptake into the pores is provided more than sufficient time (usually about two hours) to reach adsorption equilibrium. A pneumatic valve is then toggled, switching the influent to a highly convective inert helium stream (50 mL/min), and desorption from the chamber is monitored for up to two hours. All flows were controlled with Brooks 5850E mass flow controllers, and temperatures were maintained at 10 °C in the bubbler and 90 °C in the transfer lines. Back pressure before the chamber and in the bubbler was maintained at 5 psi. A modified HP 5890 GC was used to maintain isothermal chamber conditions as well as for valve control and flame ionization detection. Cyclohexane (99.9%, Fisher # C556-4), Middlesex UHP He (99.999%), UHP H_2 (99.999%), and Ultra Zero Air (<2 ppm H_2O) were used in all experiments. The vapor pressure of cyclohexane was maintained at 2.3 Torr during uptake.

3.0. ZERO LENGTH CHROMATOGRAPHY

ZLC was developed by Ruthven and Brandani and extensively used for measuring mass transport in microporous materials.[39] The widely used model, described here as the "base model", and several mechanistic models accounting for surface barriers are presented and summarized in Table 2. All models examined here assume "spherical" geometries due to the three-dimensionally interconnected pore network of MFI, as is assumed in the literature for the silicalite-1 system[40] and confirmed in the Supporting Information by using the method of Cavalcante et al.[43]

3.1. Base Model. The base ZLC model assumes mass transport is controlled entirely by bulk diffusion. Starting with a one-dimensional, radial mass balance around a zeolite particle for a transient system, the boundary value problem can be summarized by

Governing Equation:

$$\frac{dq}{dt} = D\nabla_r^2 q \tag{1}$$

Initial Condition:

$$q(r, t = 0) = q_0 = Kc_0 \tag{2}$$

Boundary Conditions:

$$\left.\frac{\partial q}{\partial r}\right|_{r=0} = 0 \tag{3}$$

$$-D\left.\frac{\partial q}{\partial r}\right|_{r=R} = \frac{FR}{3KV_s}q_R = \frac{FR}{3V_s}c \tag{4}$$

where q is the surface concentration; D is the intracrystalline diffusivity; and c is the gas-phase concentration. At equilibrium, q is directly related to c by the proportionality constant, K (Henry's constant). F is the flow rate of gas into the sample chamber with crystals of radius R and total adsorbent volume of V_s. The second boundary condition arises from balancing the fluxes at the surface between the bulk gas phase and the equilibrium surface concentration.

The solution to the transient, three-dimensional (spherical) desorption profile in the diffusion controlled regime ($L > 10$) has been solved analytically by Ruthven and Brandani[39,44]

$$\frac{c}{c_0} = \sum \frac{2L}{\beta_n^2 + (1 - L + \gamma\beta_n^2)^2 + L - 1 + \gamma\beta_n^2} \times \exp\left(-\beta_n^2 \frac{D_{app}}{R^2}t\right) \tag{5}$$

where

$$\beta_n \cot \beta_n + L - 1 - \gamma\beta_n^2 = 0 \tag{6}$$

and

$$L = \frac{\tau_{Diff}}{\tau_{washout}} = \frac{1}{3}\frac{F}{KV_s}\frac{R^2}{D} \tag{7}$$

L represents the ratio of diffusional time through the bulk to the washout time in which the bulk gas accumulated in the cell and weakly physisorbed surface-bound molecules deplete from the sample chamber. For gaseous systems, holdup in the sample chamber is often neglected, and gamma is taken as zero.

$$\gamma = \frac{1}{3}\frac{V_f}{KV_s} \cong 0 \tag{8}$$

A two-parameter least-squares nonlinear fit is performed on the system of eqs 5−7, minimizing the logarithmic error between the experimental desorption profile and eq 5 to determine D and L.

3.2. Surface Resistance Model. The base model can be expanded upon by accounting for physical phenomena at the surface. Several researchers have attempted to broadly describe the surface effect by introducing a surface mass transfer limitation that accounts for hindered transport across the surface of a zeolite.[32,36] In the ZLC model, this has been implemented by resolving the second boundary condition by balancing internal flux ($J_{in} = -D\nabla_r q = -D(\partial q/\partial r)|_R$) with a resistive flux near the surface ($J_{surf} = k_s(q_R - q_{surf})$). In this case, a surface barrier is assumed to arise from restricted diffusion through a thin layer just below the surface and is described by the mass transfer coefficient, k_s. Assuming equilibrium between the surface of the particle and the external bulk gases, the second boundary condition becomes

$$-D\left.\frac{\partial q}{\partial r}\right|_R = k_s(q_R - q_{surf}) = \frac{FR}{3V_s}c = \frac{FR}{3KV_s}q_{surf} \tag{9}$$

The boundary value problem is then defined by eqs 1−3 and 9.

The solution is identical to eqs 5−8 with the exception that the parameter L is redefined by

$$L' = \frac{\tau_{diff}}{\tau_{washout} + \tau_{surf}} = \frac{R^2/3D}{KV_s/F + R/k_s} \tag{10}$$

where L' now represents the ratio of the diffusional time constant to the combined washout and first-order mass transfer limitation time constant at the surface.

3.3. Kinetic Desorption Model. A more mechanistic model can be applied to the surface boundary by assuming that desorption from a surface site to the bulk becomes rate limiting and the surface is no longer in equilibrium with the bulk gas ("base" and "surface resistance" models). In the situation where desorption on the outer surface of the particle is potentially rate limiting, the boundary condition can again be modified by performing a flux balance at the surface, equating internal diffusion flux ($J_{in} = -D\nabla_r q = -D(\partial q/\partial r)|_R$) to the first-order

dx.doi.org/10.1021/jp4089595 | J. Phys. Chem. C 2013, 117, 25545−25555

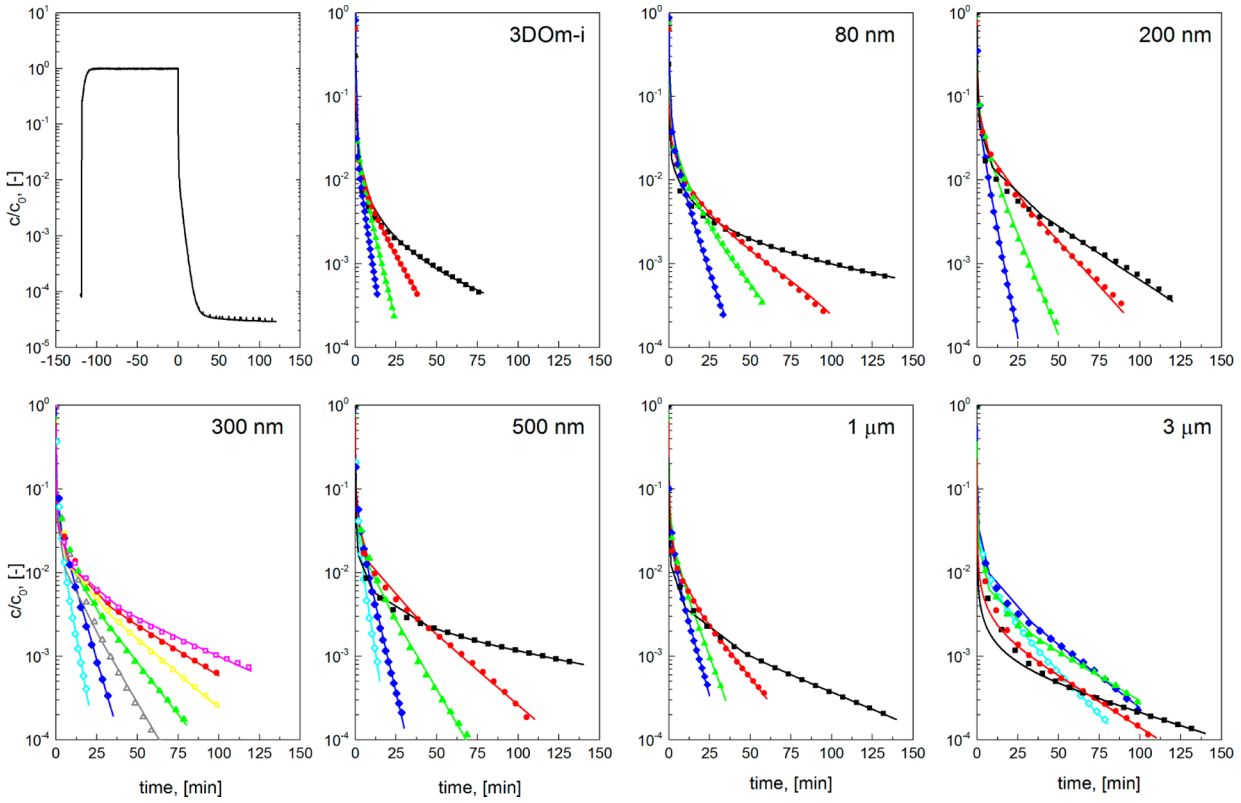

Figure 4. Cyclohexane/silicalite-1 desorption profiles. Isothermal diffusion desorption curves (data points) and model fits (solid curves). T = 50 °C (black filled box), 60 °C (pink outlined box), 70 °C (red filled circle), 80 °C (yellow outlined circle), 90 °C (green filled triangle), 100 °C (gray outlined triangle), 110 °C (blue filled diamond), 130 °C (blue outlined diamond).

desorption flux ($J_{des} = (k_{des}R/3)q_R$), giving rise to the boundary condition

$$-D\frac{\partial q}{\partial r}\bigg|_R = \frac{k_{des}R}{3}q_R = \frac{FR}{3V_s}c \tag{11}$$

The boundary value problem is similarly defined by eqs 1−3 and 11.

The solution is identical to eqs 5−8 with the exception that the parameter L is redefined by

$$L'' = \frac{\tau_{Diff}}{\tau_{des}} = \frac{R^2/3D}{1/k_{des}} \tag{12}$$

where L'' now represents the ratio of intracrystalline diffusion time to the desorption time constant.

3.4. Intracrystalline Verification. Intracrystalline transport was verified as rate limiting under experimental conditions by several quantitative and experimental measures. For brevity, the four criteria are outlined here and described in greater detail in the Supporting Information.

A. **Uptake Condition.** Sufficient time[41] for uptake of the adsorbate (cyclohexane) was provided to allow the crystal to fully equilibrate with the dilute gas stream.

B. **Macroscopic Measurability Condition.** To ensure that the concentration of the gas-phase diffusing species was within detection limits, the minimum time scale for diffusion was calculated to be sufficiently high to attain a measurable desorption profile. This was assessed for the diffusion rates of interest and for the maximum detector sampling frequency.

C. **Internal Transport Condition.** The use of ZLC requires that the rate-controlling step is intracrystalline diffusion, not external mass transfer. In the cyclohexane/silicalite-1 system, for the range of temperatures analyzed, the condition is easily satisfied, ranging from $10^7 < \tau_{Diff}/\tau_{ext} < 10^9$, indicating that all considered experiments are limited by internal transport ($\tau_{Diff}/\tau_{ext} \gg 5$).

D. **Kinetic Transport Control.** If the residence time in the sample chamber is too high or the adsorbate is too strongly adsorbed to the surface, the system may be under equilibrium control. The kinetic transport control condition was assessed by calculating L'', which describes the ratio of diffusion time constant to desorption time. The condition was also confirmed experimentally by monitoring the parameter L (the measure of diffusion time to external transport), which ranged from $10 < L < 500$.

The experimental ZLC data obtained in this study were validated against all four criteria, and intracrystalline diffusion was shown to be rate limiting in the cyclohexane/silicalite-1 system at 2.3 Torr saturation pressure and T = 50−250 °C for the considered particle sizes.

4.0. RESULTS AND DISCUSSION

ZLC desorption curves for all considered particles and temperatures are presented along with model fits in Figure 4. In all cases, there was strong agreement between the two-parameter model fit (D_{app} and L) and experimental desorption curves. L values for all conditions were always above 10, indicating internal particle transport limitations, and average diffusivity values of three runs per data point are reported in Figure 5.

The apparent diffusivity, D_{app}, represents the macroscopically observed diffusivity through the particle. It is calculated by

dx.doi.org/10.1021/jp4089595 | J. Phys. Chem. C 2013, 117, 25545−25555

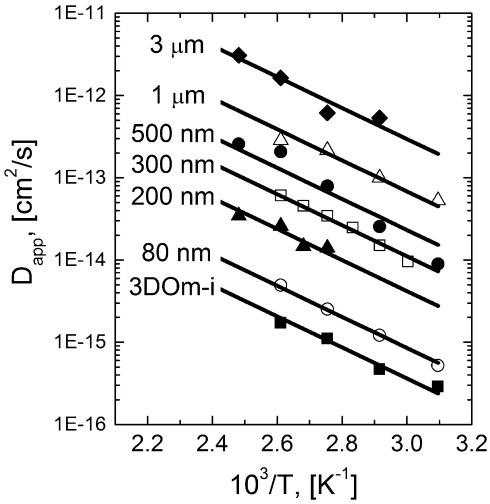

Figure 5. Cyclohexane/silicalite-1 Arrhenius plot. Experimentally observed diffusion coefficients conform to the Arrhenius relationship, exhibiting constant activation energy and significantly different pre-exponential factors. Nominal sizes: 3DOm-i (■), 80 nm (○), 200 nm (▲), 300 nm (□), 500 nm (●), 1 μm (Δ), 3 μm (♦).

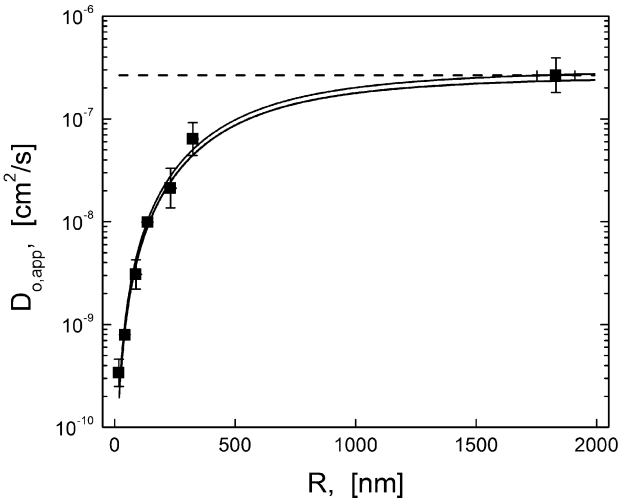

Figure 6. Apparent diffusivity pre-exponential and model fits. The pre-exponential to the apparent diffusivity (■) is observed to decrease over orders of magnitude as particle size becomes smaller. Models for pore narrowing (black —) and pore blockage (gray —) appear to fit the experimental data, while the kinetic surface desorption mechanism (---) does not.

dividing the square of the diffusional length scale, R, by the diffusional time constant from eq 5 ($\tau = R^2/D_{app}$). The diffusion coefficient is known to be temperature activated in accordance with the Arrhenius relationship[16]

$$D = D_0 \exp\left(-\frac{E_a}{\mathcal{R}T}\right) \tag{13}$$

where the activation energy, E_a, is the energy required by a diffusing molecule to jump between lattice cages to perform the rate-limiting transport step. Because all silicalite-1 particles exhibit identical porous structure, E_a should be constant for all silicalite-1 particle sizes.[16] This behavior is consistent with the systems studied here where the Arrhenius slopes are statistically equal for all the particles as presented in Figure 5. Solid lines represent constant activation energy fits, where the constant activation energy was taken to be the arithmetic mean of the seven samples (E_a = 38 ± 4 kJ/mol). This is in the range of literature values of the intracrystalline activation energy which utilizes several experimental techniques to obtain values of 56.6,[24] 33.8,[45] 26.4,[46] 64.8,[47] 50.6,[48] and 53.5[49] kJ/mol.[24] In this work, no significant trend was observed between the apparent activation energy and particle size, indicating a common transport mechanism through all particle sizes that is not enthalpically different from transport within the bulk of the particle.

Values of the pre-exponential appear to asymptotically approach a constant value as particle size increases (Figure 6), corresponding to bulk diffusion coefficients for large particles in the range of those previously reported in the literature.[40] As represented in Supporting Information Figure S2, diffusivity values for large particles (R = 1, 3 μm) in this study correspond well with those measured previously in the literature (R = 3, 7, 50 μm), which is believed to represent bulk intracrystalline diffusion.

Interestingly, the apparent pre-exponential factor, D_0, is not constant; it decreases over 3 orders of magnitude as particle size decreases (Figure 6). The contribution of the apparent pre-exponential to the overall apparent diffusivity appears to be responsible for the drastic decreases in diffusion coefficients observed in small particles in Figure 6. The pre-exponential factor of the Arrhenius form of the diffusion coefficient has been interpreted to be the entropic contribution in transition state theory[16,29,50]

$$D_0 = \frac{a^2\omega(T)}{2\pi} \exp\left(-\frac{\Delta S(T)}{k_B}\right) \tag{14}$$

with the lattice dimensions (a), site vibrational frequency (ω), and entropy of a lattice step. Because these parameters all depend on the adsorbate/host interaction and do not vary with respect to particle size, the pre-exponential factor should remain constant. As there is a strong dependence on particle sizes here (Figure 5 and Figure 6), a different mechanistic explanation is necessary to justify the divergence in diffusivity values for small particles.

The precipitous reduction in apparent diffusion coefficients with smaller particle sizes indicates the presence of a second transport phenomenon dependent on particle size. The two broad classes of mechanistic justification discussed here are internal grain boundaries and surface barriers. Several mechanisms focus on the surface, suggesting either an entropic effect associated with the reorientation or tortuosity of the diffusing molecule at the surface[51,52] or an extension of the diffusional length scale near the surface.[36,53] Each proposed secondary rate limitation is discussed and evaluated in the subsequent sections for their ability to describe the particle size dependence of the experimentally determined diffusion coefficients.

4.1. Internal Grain Boundaries. Boundaries that exist at the crystalline interface within zeolites (internal grain boundaries) are considered to be a possible cause for mass transfer limitations to intracrystalline diffusion. In the MFI coffin-shaped crystal, ordered grain boundaries exist that are believed to hinder internal diffusion by causing discontinuous pore channels.[54,55] It is proposed that the presence of these barriers, which can be either impermeable or semipermeable, significantly reduces adsorbate flux through the particle on a macroscopic scale.[22,54] Vasenkov et al. performed kinetic

dx.doi.org/10.1021/jp4089595 | J. Phys. Chem. C 2013, 117, 25545−25555

Monte Carlo simulations and PFG−NMR diffusion studies through MFI and suggested that the outer surface does not play a significant role in apparent diffusion.[56,57] Instead, the authors suggest the presence of permeable grain boundaries and intergrowths as diffusion limitations. These internal blockages were observed experimentally using a combination of spectroscopic, scattering, and microscopy techniques, where accumulation of diffusing molecules at grain boundaries was observed with pore misalignments at angles as small as 0.5−2°.[54]

In addition to grain boundaries, intergrowths or crystal defects within the MFI structure have also been suggested as responsible for macroscopically observed diffusion barriers.[58,59] These internal barriers result from the synthesis process and are believed to cause regular defects. While the presence of internal crystal defects not ordered on a crystal grain boundary (intergrowths) may be responsible for a decrease in transport time through the particle, the dependence of the diffusivity on particle size suggests it is not responsible for the strong size dependence observed in the transport rate.

4.2. Surface Barriers. A "surface barrier" is a general term for any resistance to mass transfer at or near the surface of a zeolite pore. While the mechanism contributing to a surface mass transport limitation has not been conclusively identified, surface barriers in small particles have been claimed to account for up to 60% of overall mass transfer.[24] The surface barrier phenomenon has been explained by numerous mechanisms including surface coking, strongly adsorbed diffusing molecules, accumulation near pores, strongly bound water molecules, a slow kinetic desorption step, pore narrowing, and total pore blockages.[18,24,25,32,36,50,51,60−64]

The simplest analysis of surface barriers assumes a mass transfer coefficient at the particle surface to describe an undefined mechanism.[24,32,65] In these models, bulk diffusion is assumed to describe transport in the internal crystal domain, while desorption from the surface to the bulk gas is assumed to be in equilibrium. Unlike the traditional solution, however, an intermediary transport step is introduced in which a mass transfer resistance ($\tau_m = 1/k_m$) exists between the bulk crystal and the surface.

Three specific mechanisms for surface barriers are presented, discussed, and evaluated here in an attempt to determine the origin of the secondary transport limitation. The mechanisms considered are qualitatively described in Figure 7 and summarized mathematically in Table 2: narrowing of the pores at the surface (Mechanism I); extension of the diffusional length scale near the surface due to total pore blockages (Mechanism II); and desorption of molecules from the surface to the bulk gas phase (Mechanism III). Full derivations for each mechanism are provided in the Supporting Information.

Surface Pore Narrowing (I). It is possible to explain surface barrier limitations as a step through the surface that is slower than the bulk due to surface pore narrowing. A comprehensive study on the morphology of MFI crystals has identified a "crust" on the outer surface of particles, 10−200 nm in thickness, resulting from the synthesis process.[54] This crust is believed to be responsible for mass transport rate limitations due to inherent structural difference through the layer.

Lercher and co-workers have proposed that a transport step at the surface that is enthalpically different from the bulk can be rate limiting in small crystals.[66] The authors describe overall diffusion through the particle as a series of three kinetic steps: adsorption to the surface, diffusion into a surface defect layer,

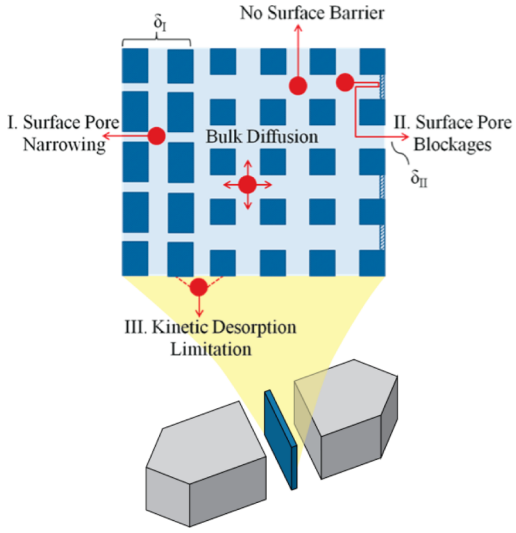

Figure 7. Qualitative visualization of surface barriers. Mechanistic transport across the zeolite surface is described as either having no transport barrier, surface pore narrowing (I), surface pore blockages (II), or kinetic desorption limitations (III).

and bulk diffusion into the crystal. In large particles (>3 μm), model predictions fit to frequency response data identify bulk crystal diffusion control, while small particles (<100 nm) are proposed to be limited by either transport across the surface or desorption from the surface to the bulk gas phase. Gueudré et al. studied diffusion of cyclohexane in two different sizes of MFI crystals and qualitatively report a temperature-activated surface barrier effect different from bulk diffusion.[24]

In our study, an additive mechanistic model is proposed and quantitatively compared to experimentally observed diffusion coefficients for several temperatures. In this model, a finite crust of length δ_I is assumed to penetrate into the surface of the particle. The apparent time scale is then assumed to be a linear combination of the two transport time scales, namely, bulk diffusion and diffusion through the surface

$$\tau_{app} = \frac{R^2}{D_{app}} = \tau_{bulk} + \tau_s \tag{15}$$

where $\tau_{bulk} = R_{bulk}^2/D$ is the time scale for diffusion through the bulk; $\tau_s = \delta_I^2/D_s$ is the time scale through the crust; and $R = R_{bulk} + \delta_I$. In this case, pore narrowing is represented mechanistically by a diffusion constant different from that of the bulk ($D_s \neq D$). Applying the Arrhenius relationship to relate the apparent pre-exponential to the surface length scales, the apparent pre-exponential can be algebraically solved to obtain

$$D_{0,app} = R^2 \times \left[\frac{(R-\delta_I)^2}{D_0}\exp\left(\frac{E_{Diff} - E_{app}}{\mathcal{R}T}\right) + \frac{\delta_I^2}{D_{0,s}}\exp\left(\frac{E_s - E_{app}}{\mathcal{R}T}\right)\right]^{-1} \tag{16}$$

This description implies that the slope of the Arrhenius curves should change with particle size. However, as observed in this work and the literature, no dependence of E_{app} on particle size is observed, and the activation energies associated with transport through the surface, E_s, and bulk appear to be equal.

dx.doi.org/10.1021/jp4089595 | J. Phys. Chem. C 2013, 117, 25545−25555

In the case of pore narrowing, diffusion through a crust (or across a single layer) is hindered by an entropic surface effect such as a reorientation of a molecule at the pore surface.[51,67] On the basis of the constant activation energy observed experimentally (in Figure 6), with the assumption that $E_{Diff} = E_s = E_{app}$, eq 16 reduces the entropic contribution to the apparent pre-exponential to diffusion

$$D_{app,0} = R^2\left[\frac{(R-\delta_I)^2}{D_0} + \frac{\delta_I^2}{D_{s,0}}\right]^{-1} \quad (17)$$

where the bulk pre-exponential factor, D_0, is taken to be the asymptotic value for large particles, $D_0 = 2.7 \times 10^{-7}$ cm^2/s. The model fit then reduces to the two parameters: penetration depth of the surface barrier, δ_I, and the pre-exponential factor for diffusion across the barrier, $D_{s,0}$. The model can be fit with the experimental data set $D_{app,0}(R)$, and the resulting fit is represented in Figure 6. The predicted crust penetration depth is estimated as $\delta_I = 25$ nm.

A surface crust thickness of 25 nm is reasonable when compared to known structural differences observed penetrating into the surface of MFI (10−200 nm).[54] The pore narrowing model predicts a hindered diffusion coefficient at the surface with $D_0 = 3.4 \times 10^{-10}$ cm^2/s. In this model, this extremely slow diffusivity results entirely from the pre-exponential to the diffusion coefficient in the Arrhenius relationship.

Pore Blockage (II). An alternative theory for surface barriers examines the possibility of physical blockages of surface pores. Pore blockages cause an extension of the diffusional length scale due to the additional path a molecule must travel to locate an open surface pore. Support for the surface pore blockage theory has arisen from experiments measuring diffusivity across modified zeolite surfaces by surface etching with hydrofluoric acid[24,68] and deposition of an amorphous surface layer via silylation.[36,69] Pore blockage at the surface was also proposed by Reitmeir et al., who claimed that the absence of variation in activation energy associated with the Arrhenius form of diffusivity, D, supports only closed pores; in their view, pore restriction should alter the activation energy in the surface region.[29] Brandani studied the correlation between diffusivity and displacement of *n*-alkanes in silicalite-1 across several length scales and concluded that smaller diffusivities were likely caused by a longer diffusional path, not a slower diffusion rate.[20] This is important because it means that the self-diffusivity, which represents a single molecule jumping through the lattice, remains constant, while the apparent (transport) diffusivity across the entire particle is observed to be slower.

Blockage of pores at the zeolite particle surface will lead to longer diffusion paths and apparent transport length scales. It also suggests that a surface pore blockage effect should be more pronounced in smaller particles where the additional path length needed for a diffusing molecule to find an open pore becomes comparable to the bulk transport length scale (particle diameter). Kärger and co-workers developed an interference microscopy technique that allowed for spatially and temporally resolved concentration profiles of single zeolite particles.[22,71,77] In this work, the authors are able to decouple bulk diffusion and surface permeability in metal organic frameworks (MOFs).[61,70,71] An accumulation of diffusing molecules is observed at the surface; however, the permeability across the surface was shown to exhibit the same activation energy as the bulk, indicating the same fundamental transport step.[61] Because the activation energy remains constant, the mechanisms for the bulk and surface are likely the same, again indicative of diffusion control across the surface, likely due to surface pore blockages.

In this work, mechanistic evaluation is provided to assess the possibility of pore blockages in silicalite-1. As with the pore narrowing mechanism, the observed transport time is assumed to be an additive combination of the bulk transport ($\tau_{bulk} = R^2/D$) and diffusion across the surface barrier ($\tau_s = \delta_{II}^2/D$). In this case, the diffusion constants through the bulk and the surface are both assumed to be identical, and eq 15 can be solved for the apparent pre-exponential

$$D_{app,0} = D_0\left[1 + \left(\frac{\delta_{II}}{R}\right)^2\right]^{-1} \quad (18)$$

Relaxing the constraint that D_0 must be the asymptotic value, the model fit shown in Figure 6 predicts parameters ($D_0 = 3.1 \times 10^{-7}$) cm^2/s and $\delta_{II} = 740$ nm. The first parameter, D_0, predicts an intracrystalline diffusivity pre-exponential similar to that predicted earlier for the bulk ($D_{0,bulk} = 2.7 \times 10^{-7}$), which is consistent with the theory that the diffusivity remains constant, while the diffusional length scale increases in smaller particles. The additional diffusion length of 740 nm represents the additional distance a molecule must travel to locate an open surface pore. In situations where the fraction of surface pore blockages is significant, the additional length can be larger than the particle itself. In conclusion, pore blockage agrees well with the experimental results and offers an explanation for the observed secondary transport limitation.

Surface Desorption (III). The final surface barrier mechanism evaluates slow surface desorption relative to bulk diffusion. By this mechanism, adsorbates can rapidly diffuse to the particle surface, but they are blocked from exiting the pore by high surface coverage on the external particle surface. In zeolite membranes and small crystals where little or no bulk lattice exists, it may be possible to be transport limited by desorption from the surface to the bulk gas phase.[16,72] This theory was first presented by Barrer et al. who described a surface evaporation step;[73,74] however, it has yet to be supported experimentally.[75,76] The possibility of a desorption limitation was considered at steady state by Kärger and co-workers[16] who determined that, under desorption control ($k_{des} \ll D/R^2$), the time scale becomes dominated by the desorption time, $\tau_s = 1/k_{des}$, and the time scale associated with transport to the bulk phase from the surface (permeability) is expected to be independent of particle size. While the desorption step presumes a difference in activation energy as the elution process transitions from bulk diffusion (E_{Diff}) to desorption (ΔH_{des}), mechanisms such as this cannot be discounted; the activation energy for cyclohexane diffusion in silicalite-1 (E_a = 26 − 56 kL/mol[40]) has been reported to be similar to the heat of desorption ($-\Delta H_{ads} = 57.3$ kJ/mol[40]).

The desorption limitation mechanism is evaluated assuming additive time scales (eq 15), where the time scale for a molecule to desorb from the surface to the bulk gas phase is $\tau_s = 1/k_{des}$. In this case, both the bulk diffusion coefficient and the kinetic desorption constant are assumed to be temperature activated according to the Arrhenius and Polanyi−Wigner[77] relationships ($k_d = k_{des,0}\exp(-E_{des}/RT)$), respectively. Assuming that the desorption energy is equal to the enthalpy of desorption, $E_{des} \approx -\Delta H_{ads} \neq E_{Diff}$, and the desorption rate is first order, the pre-exponential factor of the Arrhenius form of the apparent diffusion coefficient, D_{app}, becomes

dx.doi.org/10.1021/jp4089595 | J. Phys. Chem. C 2013, 117, 25545−25555

$$D_{app,0} = \frac{k_{des,0} D_0}{k_{des,0} \exp\left(\frac{E_{Diff} - E_{app}}{\mathcal{R}T}\right) + \frac{D_0}{R^2} \exp\left(\frac{-\Delta H_{ads} - E_{app}}{\mathcal{R}T}\right)} \quad (19)$$

where $k_{des,0}$ is the frequency factor for the first-order desorption rate constant; ΔH_{ads} is taken as 57.3 kJ/mol;[40] E_{app} is the experimentally averaged activation energy (38 ± 4 kJ/mol); and the bulk diffusion parameters are again assumed to be the asymptotic value observed in large particles ($D_0 = 2.7 \times 10^{-7}$ cm^2/s, $E_{diff} = 38$ kJ/mol). The pre-exponential in the Polanyi–Wigner relationship is taken as $k_{des,0} = 10^{13}$ s^{-1}, as a common assumption for the jump frequency.[77]

In the range of temperatures examined in this study, the predicted desorption-controlled model is shown in Figure 6, where negligible dependence on particle size is observed. This is due to the extremely fast desorption step compared to bulk diffusion ($L'' = (\tau_{Diff}/\tau_{des}) \sim 10^8$–$10^9$), even in small particles. This result suggests that the system is not desorption controlled. Furthermore, for desorption to be relevant to the overall rate, either the pre-exponential, $k_{des,0}$, would have to be many orders of magnitude smaller or the difference between the enthalpy of desorption ($-\Delta H_{ads}$) and the activation energy for diffusion ($E_{a,diff}$) would need to be substantially larger, which literature has suggested is not the case.[40]

4.3. Implications. New hierarchical microporous materials with ordered or disordered mesoporosity are currently being synthesized with microporous frameworks and particle length scales as thin as single unit cells.[7,11] However, surface barriers have been shown here to be prevalent and even dominant in small zeolite particles and are likely due to structural differences/defects of pores at or near the surface. In preparation and characterization of such materials, special consideration should be made to ensure structurally pure zeolite surfaces with unhindered transport due to substantial surface defects. As the surface appears exceptionally important and susceptible to blockages/restrictions in small particles, protection of the surface from unnecessary exposure to chemical or mechanical blockages by development of ordered, mesoporous, or templated materials is necessary to maximize the turnover potential of hierarchical materials.

CONCLUSIONS

Direct evidence is presented to support secondary, size-dependent transport limitations in small microporous particles. A set of well-defined silicalite-1 particles was synthesized of known size spanning 3 orders of magnitude, and apparent diffusion coefficients of cyclohexane/silicalite-1 were measured by zero length chromatography. Arrhenius temperature dependence of measured apparent diffusivities confirmed that all particles were temperature activated with the same activation energy. However, the pre-exponential factor for the apparent diffusion constant was observed to decrease over 3 orders of magnitude as particle size decreased. Variation in apparent diffusivity was examined by three mechanisms including surface pore constriction, surface pore blockage, and surface desorption of cyclohexane. While desorption of cyclohexane was insufficient to explain the drastic reduction of apparent cyclohexane diffusivity in small particles, surface pore constriction/blockage was viable.

ASSOCIATED CONTENT

Supporting Information

Detailed validation of the ZLC system as well as analytical derivations of the mechanistic surface barrier models. This material is available free of charge via the Internet at http://pubs.acs.org.

AUTHOR INFORMATION

Corresponding Authors

*E-mail: dauenhauer@ecs.umass.edu.
*E-mail: wfan@ecs.umass.edu.

Notes

The authors declare no competing financial interest.

ACKNOWLEDGMENTS

This work was supported in part by the Catalysis Center for Energy Innovation, an Energy Frontier Research Center funded by the U.S. Department of Energy, Office of Science, Office of Basic Energy Sciences under Award Number DE-SC0001004. Andrew Teixeira was partially supported by a subcontract with Cornell University, Department of Biological and Environmental Engineering, under Prime Agreement Award Number DTOS59-07-G-00052 from the United States Department of Transportation, Office of the Secretary. The authors would like to acknowledge Professors Wm. Curt Conner and Michael Tsapatsis for their valuable insight into adsorption and diffusion in zeolites.

NOMENCLATURE

a = Length of a single lattice step
c = Gas-phase effluent concentration
q = Adsorbate surface concentration
D, D_{app} = Intracrystalline diffusion coefficient and apparent diffusion coefficient
D_0, $D_{app,0}$, $D_{s,0}$ = Arrhenius pre-exponential factor for intracrystalline, apparent, and surface diffusion, respectively
E_{Diff}, E_{app}, E_s = Activation energies for diffusion, apparent diffusion, and surface barriers
F = Convective volumetric flow rate through the diffusion chamber
ΔH_{ads} = The heat of adsorption of a molecule adsorbing to the surface of a zeolite
K = Dimensionless equilibrium constant (Henry's constant)
k_B = Boltzmann's constant, 1.3806×10^{-23} J/K
k_{des} = First-order kinetic desorption rate constant
k_s = First-order mass transfer coefficient
L, L', L'' = Ratio of diffusional time to secondary transport time constant (eqs 7, 10, 12)
r = Spacial coordinate in spherical particle
R = Diffusional length scales in spherical coordinates, $R = (lwh)^{1/3}$
$\mathcal{R}$ = Ideal gas constant, 8.314 J mol^{-1} K^{-1}
ΔS = Entropy change associated with a molecule diffusing into a micropore
t = Desorption time
V_f = Fluid volume
V_s = Adsorbent volume
β_n = Infinite series defined by eq 6
γ = Ratio of accumulation in the fluid to the solid, defined by eq 8
δ_I, δ_{II} = Surface barrier length scales for (I) crust and (II) additional diffusion length

τ = Transport time constant
ω = Vibrational frequency of an adsorbed molecule on a zeolite

REFERENCES

(1) Csicsery, S. M. Shape-Selective Catalysis in Zeolites. *Zeolites* **1984**, *4*, 202−213.
(2) Corma, A. Inorganic Solid Acids and Their Use in Acid-Catalyzed Hydrocarbon Reactions. *Chem. Rev.* **1995**, *95*, 559−614.
(3) Young, L. B.; Butter, S. A.; Kaeding, W. W. Shape Selective Reactions with Zeolite Catalysts, iii. Selectivity in Xylene Isomerization, Toluene Methanol Alkylation, and Toluene Disproportionation over ZSM-5 Zeolite Catalysts. *J. Catal.* **1982**, *76*, 418−432.
(4) Jobic, H.; Schmidt, W.; Krause, C. B.; Kärger, J. PFG NMR and QENS Diffusion Study of n-Alkane Homologues in MFI-Type Zeolites. *Microporous Mesoporous Mater.* **2006**, *90*, 299−306.
(5) van den Bergh, J.; Gascon, J.; Kapteijn, F. Diffusion in Zeolites − Impact on Catalysis. In *Zeolites and Catalysis*; Wiley-VCH Verlag GmbH & Co. KGaA: Weinheim, Germany, 2010; pp 361−387.
(6) Watanabe, R.; Yokoi, T.; Tatsumi, T. Synthesis and Application of Colloidal Nanocrystals of the MFI-Type Zeolites. *J. Colloid Interface Sci.* **2011**, *356*, 434−441.
(7) Fan, W.; Snyder, M. A.; Kumar, S.; Lee, P.-S.; Yoo, W. C.; McCormick, A. V.; Lee Penn, R.; Stein, A.; Tsapatsis, M. Hierarchical Nanofabrication of Microporous Crystals with Ordered Mesoporosity. *Nat. Mater.* **2008**, *7*, 984−991.
(8) Lee, P.-S.; Zhang, X.; Stoeger, J. A.; Malek, A.; Fan, W.; Kumar, S.; Yoo, W. C.; Al Hashimi, S.; Penn, R. L.; Stein, A.; Tsapatsis, M. Sub-40 nm Zeolite Suspensions via Disassembly of Three-Dimensionally Ordered Mesoporous-Imprinted Silicalite-1. *J. Am. Chem. Soc.* **2010**, *133*, 493−502.
(9) Na, K.; Jo, C.; Kim, J.; Cho, K.; Jung, J.; Seo, Y.; Messinger, R. J.; Chmelka, B. F.; Ryoo, R. Directing Zeolite Structures Into Hierarchically Nanoporous Architectures. *Science* **2011**, *333*, 328−332.
(10) Choi, M.; Na, K.; Kim, J.; Sakamoto, Y.; Terasaki, O.; Ryoo, R. Stable Single-Unit-Cell Nanosheets of Zeolite MFI as Active and Long-Lived Catalysts. *Nature* **2009**, *461*, 246−249.
(11) Zhang, X.; Liu, D.; Xu, D.; Asahina, S.; Cychosz, K. A.; Agrawal, K. V.; Al Wahedi, Y.; Bhan, A.; Al Hashimi, S.; Terasaki, O.; Thommes, M.; Tsapatsis, M. Synthesis of Self-Pillared Zeolite Nanosheets by Repetitive Branching. *Science* **2012**, *336*, 1684−1687.
(12) Tiselius, A. Adsorption and Diffusion in Zeolite Crystals. *J. Phys. Chem.* **1936**, *40*, 223−232.
(13) Auerbach, S. M.; Carrado, K. A.; Dutta, P. K. *Handbook of Zeolite Science and Technology*; M. Dekker: New York, 2003.
(14) Brandani, S.; Caro, J.; Yang, X.; Jobic, H.; Kärger, J.; Lercher, J.; Jentys, A.; Staudt, R.; Möller, A.; Ruthven, D.; Shah, D. B.; Schmidt, W. *Recent Developments in the Measurement of Diffusion in Zeolites*. FOA9 9th International Conference on Fundamentals of Adsorption. May 20−25, 2007, Sicily, Italy.
(15) Kärger, J.; Ruthven, D. M. *Diffusion in Zeolites and Other Microporous Solids*; Wiley: New York, 1992.
(16) Auerbach, S. M.; Kärger, J.; Vasenkov, S. *Diffusion in zeolites*; Marcel Dekker Inc.: New York, 2003.
(17) Kärger, J. Measurement of Diffusion in Zeolites—A Never Ending Challenge? *Adsorption* **2003**, *9*, 29−35.
(18) Ruthven, D. Diffusion in Zeolites—A Continuing Saga. *Adsorption* **2010**, *16*, 511−514.
(19) Krishna, R. Describing the Diffusion of Guest Molecules Inside Porous Structures. *J. Phys. Chem. C* **2009**, *113*, 19756−19781.
(20) Brandani, S.; Caro, J.; Jobic, H.; Kärger, J.; Krause, C.; Staudt, R. Diffusion of n-Alkanes in Zeolites: The benefit of Observation Over Different Length Scales. In *Studies in Surface Science and Catalysis*; Ruren Xu, Z. G. J. C., Wenfu, Y., Eds.; Elsevier: New York, 2007; Vol. *170*; pp 981−987.
(21) Jobic, H.; Kärger, J.; Krause, C.; Brandani, S.; Gunadi, A.; Methivier, A.; Ehlers, G.; Farago, B.; Haeussler, W.; Ruthven, D. M. Diffusivities of n-Alkanes in 5A Zeolite Measured by Neutron Spin Echo, Pulsed-Field Gradient NMR, and Zero Length Column Techniques. *Adsorption* **2005**, *11*, 403−407.
(22) Ruthven, D. M. Diffusion in Zeolites. In *Studies in Surface Science and Catalysis*; Laurent, B., Serge, K., Eds.; Elsevier: New York, 1995; Vol. *97*; pp 223−234.
(23) Brandani, S. *Macroscopic Measurement of Adsorption and Diffusion in Zeolites Adsorption and Phase Behaviour in Nanochannels and Nanotubes*; Dunne, L. J.; Manos, G., Eds.; Springer: Netherlands, 2010; pp 195−212.
(24) Gueudré, L.; Jolimaître, E.; Bats, N.; Dong, W. Diffusion in Zeolites: Is Surface Resistance a Critical Parameter? *Adsorption* **2010**, *16*, 17−27.
(25) Gobin, O. C.; Reitmeier, S. J.; Jentys, A.; Lercher, J. A. Comparison of the Transport of Aromatic Compounds in Small and Large MFI Particles. *J. Phys. Chem. C* **2009**, *113*, 20435−20444.
(26) Kocirik, M.; Struve, P.; Fiedler, K.; Bulow, M. A Model for the Mass-Transfer Resistance at the Surface of Zeolite Crystals. *J. Chem. Soc., Faraday Trans. 1* **1988**, *84*, 3001−3013.
(27) Kortunov, P.; Vasenkov, S.; Chmelik, C.; Kärger, J.; Ruthven, D. M.; Wloch, J. Influence of Defects on the External Crystal Surface on Molecular Uptake into MFI-Type Zeolites. *Chem. Mater.* **2004**, *16*, 3552−3558.
(28) Ruthven, D.; Brandani, S.; Eic, M. *Measurement of Diffusion in Microporous Solids by Macroscopic Methods Adsorption and Diffusion*; Karge, H., Weitkamp, J., Eds.; Springer: Berlin/Heidelberg, 2008; Vol. *7*; pp 45−84.
(29) Reitmeier, S. J.; Jentys, A.; Lercher, J. A. Understanding Transport in MFI-Type Zeolites on a Molecular Basis. In *Ideas in Chemistry and Molecular Sciences*; Wiley-VCH Verlag GmbH & Co. KGaA: Weinheim, Germany, 2010; pp 229−253.
(30) Agger, J. R.; Hanif, N.; Cundy, C. S.; Wade, A. P.; Dennison, S.; Rawlinson, P. A.; Anderson, M. W. Silicalite Crystal Growth Investigated by Atomic Force Microscopy. *J. Am. Chem. Soc.* **2003**, *125*, 830−839.
(31) Eić, M.; Ruthven, D. M. A New Experimental Technique for Measurement of Intracrystalline Diffusivity. *Zeolites* **1988**, *8*, 40−45.
(32) Ruthven, D. M.; Vidoni, A. ZLC Diffusion Measurements: Combined Effect of Surface Resistance and Internal Diffusion. *Chem. Eng. Sci.* **2012**, *71*, 1−4.
(33) Huang, Q.; Eić, M.; Xiao, H.; Kaliaguine, S. Characterization of the Diffusion Path in Micro- and Meso-Porous Materials from ZLC Analysis. *Adsorption* **2010**, *16*, 531−539.
(34) Malekian, A.; Vinh-Thang, H.; Huang, Q.; Eić, M.; Kaliaguine, S. Evaluation of the Main Diffusion Path in Novel Micro-Mesoporous Zeolitic Materials with the Zero Length Column Method. *Ind. Eng. Chem. Res.* **2007**, *46*, 5067−5073.
(35) Gunadi, A.; Brandani, S. Diffusion of Linear Paraffins in NaCaA Studied by the ZLC Method. *Microporous Mesoporous Mater.* **2006**, *90*, 278−283.
(36) Duncan, W.; Möller, K. Diffusion in Surface Modified ZSM-5 Studied Using the ZLC Method. *Adsorption* **2005**, *11*, 259−273.
(37) Brandani, F. *Development and Application of the Zero Length Column (ZLC) Technique for Measuring Adsorption Equilibria*; University of Maine: Orono, Maine, 2002.
(38) Eić, M.; Micke, A.; Kočirík, M.; Jama, M.; Zikánová, A. Diffusion and Immobilization Mechanisms in Zeolites studied by ZLC Chromatography. *Adsorption* **2002**, *8*, 15−22.
(39) Ruthven, D. M.; Brandani, S. Measurement of Diffusion in Porous Solids by Zero Length Column (ZLC) Methods. In *Membrane Science and Technology*; Kanellopoulos, N. K., Ed.; Elsevier: New York, 2000; Vol. *6*; pp 187−212.
(40) Duncan, W. L.; Möller, K. P. On the Diffusion of Cyclohexane in ZSM-5 Measured by Zero-Length-Column Chromatography. *Ind. Eng. Chem. Res.* **2000**, *39*, 2105−2113.
(41) Brandani, S.; Ruthven, D. M. Analysis of ZLC Desorption Curves for Gaseous Systems. *Adsorption* **1996**, *2*, 133−143.
(42) Eić, M.; Ruthven, D. M. Intracrystalline Diffusion of Linear Paraffins and Benzene in Silicalite Studied by the ZLC Method. In

Studies in Surface Science and Catalysis; Jacobs, P. A., Santen, R. A. v., Eds.; Elsevier: New York, 1989; Vol. *49*; pp 897−905.
(43) Cavalcante, C. L.; Brandani, S.; Ruthven, D. M. Evaluation of the Main Diffusion Path in Zeolites from ZLC Desorption curves. *Zeolites* **1997**, *18*, 282−285.
(44) Brandani, S.; Ruthven, D. M. Analysis of ZLC Desorption Curves for Liquid Systems. *Chem. Eng. Sci.* **1995**, *50*, 2055−2059.
(45) Wu, P.; Debebe, A.; Ma, Y. H. Adsorption and Diffusion of C6 and C8 Hydrocarbons in Silicalite. *Zeolites* **1983**, *3*, 118−122.
(46) Ban, H.; Gui, J.; Duan, L.; Zhang, X.; Song, L.; Sun, Z. Sorption of Hydrocarbons in Silicalite-1 Studied by Intelligent Gravimetry. *Fluid Phase Equilib.* **2005**, *232*, 149−158.
(47) Xiao, J.; Wei, J. Diffusion Mechanism of Hydrocarbons in Zeolites—ii. Analysis of Experimental Observations. *Chem. Eng. Sci.* **1992**, *47*, 1143−1159.
(48) Chon, H.; Park, D. H. Diffusion of Cyclohexanes in ZSM-5 Zeolites. *J. Catal.* **1988**, *114*, 1−7.
(49) Cavalcante, C. L., Jr.; Ruthven, D. M. Adsorption of Branched and Cyclic Paraffins in Silicalite. 2. Kinetics. *Ind. Eng. Chem. Res.* **1995**, *34*, 185−191.
(50) Gobin, O. C.; Reitmeier, S. J.; Jentys, A.; Lercher, J. A. Role of the Surface Modification on the Transport of Hexane Isomers in ZSM-5. *J. Phys. Chem. C* **2011**, *115*, 1171−1179.
(51) Ford, D. M.; Glandt, E. *A Molecular Simulation Approach to Studying Mass Transfer Across Surface Barriers*; Pinnavaia, T., Thorpe, M., Eds.; Springer: US, 2002; pp 319−334.
(52) Ford, D. M.; Glandt, E. D. Steric Hindrance at the Entrances to Small Pores. *J. Membr. Sci.* **1995**, *107*, 47−57.
(53) Gupta, A.; Snurr, R. Q. A Study of Pore Blockage in Silicalite Zeolite Using Free Energy Perturbation Calculations. *J. Phys. Chem. B* **2005**, *109*, 1822−1833.
(54) Karwacki, L.; Kox, M. H. F.; Matthijs de Winter, D. A.; Drury, M. R.; Meeldijk, J. D.; Stavitski, E.; Schmidt, W.; Mertens, M.; Cubillas, P.; John, N.; Chan, A.; Kahn, N.; Bare, S. R.; Anderson, M.; Kornatowski, J.; Weckhuysen, B. M. Morphology-Dependent Zeolite Intergrowth Structures Leading to Distinct Internal and Outer-Surface Molecular Diffusion Barriers. *Nat. Mater.* **2009**, *8*, 959−965.
(55) Newsome, D. A.; Sholl, D. S. Molecular Dynamics Simulations of Mass Transfer Resistance in Grain Boundaries of Twinned Zeolite Membranes. *J. Phys. Chem. B* **2006**, *110*, 22681−22689.
(56) Vasenkov, S.; Böhlmann, W.; Galvosas, P.; Geier, O.; Liu, H.; Kärger, J. PFG NMR Study of Diffusion in MFI-Type Zeolites: Evidence of the Existence of Intracrystalline Transport Barriers. *J. Phys. Chem. B* **2001**, *105*, 5922−5927.
(57) Vasenkov, S.; Kärger, J. Evidence for the Existence of Intracrystalline Transport Barriers in MFI-Type Zeolites: A Model Consistency Check Using MC Simulations. *Microporous Mesoporous Mater.* **2002**, *55*, 139−145.
(58) Muller, G.; Narbeshuber, T.; Mirth, G.; Lercher, J. A. Infrared Microscopic Study of Sorption and Diffusion of Toluene in ZSM-5. *J. Phys. Chem.* **1994**, *98*, 7436−7439.
(59) Ruthven, D. M. Transport in Microporous Solids. In *Fluid Transport in Nanoporous Materials*; Conner, W. C., Fraissard, J. P., Division, N. P. D., Eds.; Springer in cooperation with NATO Public Diplomacy Division, 2006.
(60) Krutyeva, M.; Vasenkov, S.; Yang, X.; Caro, J.; Kärger, J. Surface Barriers on Nanoporous Particles: A New Method of Their Quantitation by PFG NMR. *Microporous Mesoporous Mater.* **2007**, *104*, 89−96.
(61) Hibbe, F.; Chmelik, C.; Heinke, L.; Pramanik, S.; Li, J.; Ruthven, D. M.; Tzoulaki, D.; Kärger, J. The Nature of Surface Barriers on Nanoporous Solids Explored by Microimaging of Transient Guest Distributions. *J. Am. Chem. Soc.* **2011**, *133*, 2804−2807..
(62) Chmelik, C.; Varma, A.; Heinke, L.; Shah, D. B.; Kärger, J.; Kremer, F.; Wilczok, U.; Schmidt, W. Effect of Surface Modification on Uptake Rates of Isobutane in MFI Crystals: An Infrared Microscopy Study. *Chem. Mater.* **2007**, *19*, 6012−6019.
(63) Ruthven, D. M. Adsorption and Desorption Kinetics for Diffusion Controlled Systems with a Strongly Concentration Dependent Diffusivity. *Diffus. Fundam.* **2007**, *6*, 51.1−51.11.
(64) Tzoulaki, D.; Schmidt, W.; Wilczok, U.; Kärger, J. Formation of Surface Barriers on Silicalite-1 Crystal Fragments by Residual Water Vapour as Probed with Isobutane by Interference Microscopy. *Microporous Mesoporous Mater.* **2008**, *110*, 72−76.
(65) Ruthven, D.; Brandani, F. ZLC Response for Systems with Surface Resistance Control. *Adsorption* **2005**, *11*, 31−34.
(66) Gobin, O. C.; Reitmeier, S. J.; Jentys, A.; Lercher, J. A. Diffusion Pathways of Benzene, Toluene and p-Xylene in MFI. *Microporous Mesoporous Mater.* **2009**, *125*, 3−10.
(67) Reitmeier, S. J.; Gobin, O. C.; Jentys, A.; Lercher, J. A. Enhancement of Sorption Processes in the Zeolite H-ZSM5 by Postsynthetic Surface Modification. *Angew. Chem., Int. Ed.* **2009**, *48*, 533−538.
(68) Gueudré, L.; Bats, N.; Jolimaître, E. Effect of Surface Resistance on Cyclohexane Uptake Curves in Silicalite-1 Crystals. *Microporous Mesoporous Mater.* **2012**, *147*, 310−317.
(69) Zheng, S.; Tanaka, H.; Jentys, A.; Lercher, J. A. Novel Model Explaining Toluene Diffusion in HZSM-5 After Surface Modification. *J. Phys. Chem. B* **2003**, *108*, 1337−1343.
(70) Heinke, L.; Tzoulaki, D.; Chmelik, C.; Hibbe, F.; van Baten, J. M.; Lim, H.; Li, J.; Krishna, R.; Kärger, J. Assessing Guest Diffusivities in Porous Hosts from Transient Concentration Profiles. *Phys. Rev. Lett.* **2009**, *102*, 065901.
(71) Gueudré, L.; Binder, T.; Chmelik, C.; Hibbe, F.; Ruthven, D. M.; Kärger, J. Micro-Imaging by Interference Microscopy: A Case Study of Orientation-Dependent Guest Diffusion in MFI-Type Zeolite Host Crystals. *Materials* **2012**, *5*, 721−740.
(72) Ramanan, H.; Auerbach, S. M. Modeling Jump Diffusion in Zeolites: I. Principles and Methods. In *Fluid Transport in Nanoporous Materials*; Conner, W. C., Fraissard, J., Eds.; Springer: Netherlands, 2006; Vol. *219*; pp 93−125.
(73) Barrer, R. M. Flow Into and Through Zeolite Beds and Compacts. *Langmuir* **1987**, *3*, 309−315.
(74) Barrer, R. M.; Rosemblat, M. A. Observations on Sorption and Desorption Kinetics of n-Hexane in Zeolite H-RHO. *Zeolites* **1982**, *2*, 231−233.
(75) Magalhães, F. D.; Laurence, R. L.; Conner, W. C. Transport of n-Paraffins in Zeolite T. *AIChE J.* **1996**, *42*, 68−86.
(76) Kärger, J.; Ruthven, D. M. On the Comparison Between Macroscopic and N.M.R. Measurements of Intracrystalline Diffusion in Zeolites. *Zeolites* **1989**, *9*, 267−281.
(77) Thomas, J. M.; Thomas, W. J. *Principles and Practice of Heterogeneous Catalysis*; Wiley: New York, 1997.